ELSEVIER

International Journal of Solids and Structures 41 (2004) 4383–4405

INTERNATIONAL JOURNAL OF SOLIDS and STRUCTURES

www.elsevier.com/locate/ijsolstr

Shear behaviour of masonry panel: parametric FE analyses

Luisa Berto [a], Anna Saetta [b,*], Roberto Scotta [a], Renato Vitaliani [a,*]

[a] *Department of Construction and Transportation, University of Padova, via Marzolo 9, 35131 Italy*
[b] *Department of Architectural Construction, Dorsoduro 2206, IUAV Venice 30123, Italy*

Received 5 November 2003; received in revised form 23 February 2004
Available online 12 April 2004

Abstract

In this paper a parametric study of shear stressed masonry panels has been carried out both by means of micro- and macro-finite element modelling. Within the framework of continuum damage mechanics, two different damage models have been used: the isotropic model to simulate the behaviour of mortar in the micro-modelling approach; the orthotropic model to reproduce the non-linear behaviour of masonry in the macro-modelling. The first approach allows to accurately capture the local response of panels under shear loading, e.g. the effect of the texture (namely stack bond or running bond) and of an applied external precompression. Moreover, the micro-modelling analyses could be applied to determine the parameters necessary to calibrate the macro-model, in view of a possible use of the micro-modelling technique as a complement to or in total alternative of experimental tests. Finally the macro-model has been applied to simulate the shear tests on masonry panels proving to be able to reproduce the global behaviour of masonry.

Keywords: Masonry panels; Orthotropic damage model; Isotropic damage model; Shear loading; Micro-model; Macro-model

1. Introduction

In many traditional structures the masonry walls play an important static role; besides withstanding vertical compressive forces they usually have to carry in-plane horizontal loads (induced e.g. by wind and earthquake, and transferred to the walls primarily via diaphragms such as floors or roofs).

Consequently the shear behaviour, as well as the failure modes of shear stressed masonry panels have been subject of many investigations during the years in a number of countries.

The present work aims to analyse the masonry structural behaviour within the framework of the continuum damage mechanic in order to take into account the non-linear constitutive law of the material. In particular, two different damage models have been used according to the two different approaches, which have been followed: the micro- and the macro-modelling.

Micro-modelling is probably the best tool available to analyse and understand the real behaviour of masonry, particularly concerning its local response. Within such an approach is possible to characterise

* Corresponding authors. Tel.: +39-049-827-5622; fax: +39-049-827-5604.
E-mail address: saetta@iuav.it (A. Saetta).

0020-7683/$ - see front matter © 2004 Elsevier Ltd. All rights reserved.
doi:10.1016/j.ijsolstr.2004.02.046

separately mortar, blocks and their interfaces, adopting suitable constitutive laws for each component, which take into account their different mechanical behaviour (Page, 1978; Ali and Page, 1988; Lofti and Shing, 1994; Lourenço, 1996; Zucchini and Lourenço, 2002; Gambarotta et al., 1995). Such a modelling procedure leads to very accurate results, but requires an intensive computational effort. To overcome this problem, Tzamtzis (1994) and Sutcliffe et al. (2001) have recently proposed a simplified micro-modelling procedure which is an intermediate approach, where the properties of mortar and the unit/mortar interface are clamped into a common element, while expanded elements are used to represent the brick units.

In the following the micro-modelling has been used to investigate the local response of shear loaded masonry panels, in particular to accurately capture the effect of the texture (namely stack bond or running bond) and of an applied external precompression.

First a simple linear analysis is performed and the numerical results for the stack bond and running bond masonry are compared with those obtained by applying the explicit formulae developed by Cecchi and Sab (2002) within the homogenization theory approach. Subsequently the same numerical tests are carried out by considering a non-linear behaviour of masonry; in such analyses the effect of an external applied precompression is investigated too.

In all the analyses the bricks are modelled by adopting a linear elastic constitutive law, whereas the non-linear behaviour of the mortar is reproduced by an isotropic damage model (Saetta et al., 1999). In such a way the damage evolution in the mortar joints can be accurately followed and the real stress distribution can be determined.

As any micro-modelling analysis, the high level of refinement required for obtaining accurate results, means an intensive computational effort (i.e. great number of degrees of freedom of the numerical model), which limits its applicability to the analysis of small elements (e.g. small laboratory specimens) or, at least, to small part structural details (e.g. Sutcliffe et al., 2001; Asteris and Tzamtzis, 2003).

When large real structures have to be studied, a different approach is needed. In particular the macro-models constitute an effective method to analyse the global response of masonry structures.

In such an approach, masonry is regarded as an equivalent material, where mortar and blocks are melted together, and appropriate relations are established between averaged masonry strains and averaged masonry stresses.

A number of such models have been developed (e.g. Papa and Nappi, 1996; Callerio and Papa, 1998; Zhuge et al., 1998; Syrmakezis and Asteris, 2001; Andreaus, 1996 etc.). Among them Lourenço (1996) has proposed a non-linear constitutive model for in-plane loaded walls based on the plasticity theory. More recently Massart et al. (2001) have developed an interesting two-dimensional anisotropic damage model in a "multiplane" framework, even if, to the knowledge of the authors, up to now no one practical application has been made.

In this work the orthotropic damage model developed by the authors (Berto et al., 2002) is adopted, where masonry is considered as an orthotropic composite with different elastic and inelastic properties along the two main directions. In order to apply this model, a preliminary calibration of the material parameters is requested.

Such a calibration can be performed in different ways: (i) from a suitable set of experimental tests on full scale masonry panels, or (ii) by considering masonry as a composite material, with the preliminary experimental assessment of the behaviour of its components (brick and mortar) as input data for the following use of a homogenization technique or of the previously mentioned micro-modelling approach.

At the actual stage of the scientific cognition, the homogenization techniques can be profitably used only in the elastic field. Whereas the using of the micro-modelling technique allows a fully characterisation of the macro-model, as it will be shown in this work, taking into account the effect of the texture and precompression, both in the elastic and post-elastic field.

As final issue, it will be demonstrated the ability of the macro-model of reproducing the shear behaviour, as well as the failure modes of shear stressed masonry panels in terms of "global response".

The first part of the paper is devoted to a brief review of the two adopted damage models with a validation example of the orthotropic model.

The second part is specifically devoted to the study of the shear behaviour of masonry by varying the texture and the precompression level. In this analysis we are limiting our attention on masonry characterised by blocks much stiffer than the mortar, which is a rather usual case in our country especially for historical masonry. Moreover only two kind of pattern bond will be analyzed, namely the running and the stack bond masonry and no attention will be given to the other kind (e.g. American Bond, Flemish Bond, English Bond,...).

It is worth noting that the running bond masonry is much more common, while the stack bond is less frequent (it is sometimes used for large cross section column). However we have chosen to compare these two textures in order to better understand the importance of the pattern bond in characterising the shear behaviour of masonry, and in particular to investigate the difference between one "good masonry" (running bond) and one "bad" (stack bond).

2. Damage model: basic assumptions

In this section a brief recall of the two continuum damage models—the isotropic model and the orthotropic one—developed by the authors and adopted in the following analyses is presented.

According to the *strain-based* formulation (Simo and Ju, 1987), the state of damage can be characterised by a fourth-order tensor $\mathbf{M}$, which allows to transform the Cauchy stress tensor $\boldsymbol{\sigma}$ into the effective stress tensor $\bar{\boldsymbol{\sigma}}$ (or vice versa) as follows:

$$\bar{\boldsymbol{\sigma}} = \mathbf{M}^{-1} : \boldsymbol{\sigma} \tag{1}$$

where $\mathbf{M}$ is generally related to the fourth-order damage tensor $\widehat{\mathbf{D}}$ by means of:

$$\mathbf{M} = [\mathbf{I} - \widehat{\mathbf{D}}] \tag{2}$$

For the isotropic one-parameter damage case, relation (1) collapses to

$$\bar{\boldsymbol{\sigma}} = \frac{\boldsymbol{\sigma}}{(1-d)} \tag{3}$$

where d is the scalar variable describing the state of damage.

2.1. Isotropic damage model

The isotropic damage model we have used in the following micro-analyses, considers two independent internal damage variables—d^+ for the tensile stresses, d^- for the compressive ones—in order to take into account the different non-linear behaviour of the material under tensile or compressive loading, as well the crack closure effect upon loading reversal. With such an assumption, the effective stress tensor is split into two components $\bar{\sigma}^+_{ij}$ and $\bar{\sigma}^-_{ij}$, related respectively to d^+ and d^-, and Eq. (3) is replaced by the following (Farja and Oliver, 1998):

$$\boldsymbol{\sigma}_{ij} = (1-d^+)\bar{\boldsymbol{\sigma}}^+_{ij} + (1-d^-)\bar{\sigma}^-_{ij} \tag{4}$$

Correspondingly, two equivalent effective tensile and compressive stresses $\bar{\tau}^+$ and $\bar{\tau}^-$ are introduced, on which the damage evolution laws are depending (e.g. Farja and Oliver, 1998; Saetta et al., 1999), according to

$$d^+ = 1 - \frac{r^+_0}{\bar{\boldsymbol{\tau}}^+} \cdot \exp\left(A^+ \cdot \left(1 - \frac{\bar{\boldsymbol{\tau}}^+}{r^+_0}\right)\right) \tag{5}$$

$$d^- = 1 - \frac{r_0^-}{\bar{\tau}^-} \cdot (1 - A^-) - A^- \cdot \exp\left[B^- \cdot \left(1 - \frac{\bar{\tau}^-}{r_0^-}\right)\right] \tag{6}$$

where r_0^+, r_0^- are the current damage thresholds which control the size of the expanding damage surfaces.

These equations reproduce respectively the softening branch of the brittle material under unidimensional tensile test and both the hardening effect of material under compression and the softening after the compressive strength achieving. The detailed description of the parameters A^-, B^- and A^+, depending on the experimental data and in particular the last one on the fracture energy G_f, can be found in the previously quoted papers.

The damage criterion adopted in this formulation is similar to the Drucker–Prager failure criterion in the triaxial compression field, with a cap—closure in the tensile field. The damage function is merely the locus of all points in the effective stress space separating the accessible from inaccessible states (Fonseka and Krajcinovic, 1981).

Fig. 1 gives the constitutive curves σ–ε for both cases of uniaxial tension and compression.

Within the framework of such an approach, two global damage indexes can be defined, similarly to that proposed by Oñate (1994). Such global damage indexes have been introduced by the authors (Saetta et al., 1999) as an useful tool for monitoring the evolution of the non-linear response of a structure up to failure, with reference both to the compressive and the tensile damaging processes:

$$D^{*-} = \frac{\int_V d^- \rho_0 \Psi_0^- \, \mathrm{d}V}{\int_V \rho_0 \Psi_0^- \, \mathrm{d}V} \tag{7}$$

$$D^{*+} = \frac{\int_V d^+ \rho_0 \Psi_0^+ \, \mathrm{d}V}{\int_V \rho_0 \Psi_0^+ \, \mathrm{d}V} \tag{8}$$

respectively, for compression and tension. They represent the weighted average of the internal damage parameter on the whole structure, by using the elastic strain energy as weight. In particular Ψ_0^+ and Ψ_0^- are the Helmholtz free energy densities (per unit mass) associated to the positive and negative part of the effective stress tensor and ρ_0 is the mass density.

2.2. Orthotropic damage model

More recently, starting from the previously recalled two-parameters isotropic model, the authors have developed a more sophisticated vectorial damage model, suitable for orthotropic brittle materials, like masonry, under plane stress conditions, i.e. Berto et al. (2002).

The main assumption of this model is that the evolution of damage can modify the intensity of the anisotropy of the material but does not alter its initial symmetries. This means that the initially orthotropic

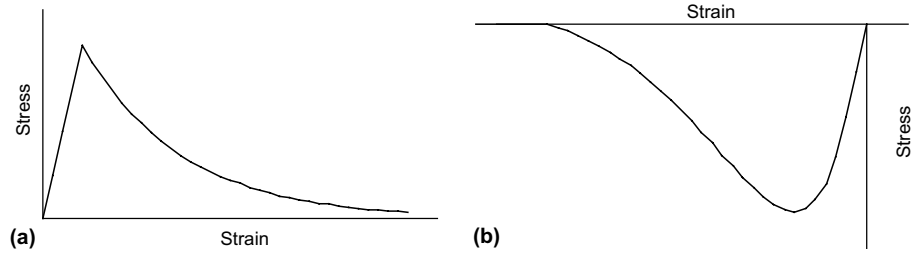

Fig. 1. Constitutive laws: (a) tension and (b) compression.

material may not evolve into more general anisotropy after the onset of damage. This assumption, together with the hypothesis of plane stress conditions, allows to simplify the theory by considering the damage variables as scalars associated with the two principal axes of the material (x–y, that are respectively the bed joint direction and the orthogonal one).

In particular, for each axis, two independent damage variables (one for tension, one for compression) are defined in order to account for the crack closure effect, similar to the isotropic model above described. In such a way four independent damage variables (d_x^+, d_x^-, d_y^+ and d_y^-) are introduced.

With these assumptions, the fourth-rank tensor $\mathbf{M}$ introduced in (1), as well as the damage tensor $\widehat{\mathbf{D}}$ whose elements are suitable functions of the damage variables and of the strain tensor, can be represented by 3×3 matrix.

In order to define the evolution laws of the damage variables and the adopted damage criterion, four independent equivalent elastic stresses $\bar{\tau}_x^+$ $\bar{\tau}_x^-$ $\bar{\tau}_y^+$ $\bar{\tau}_y^-$ (two for each natural direction of the material) have to be actually introduced. They are linear combinations of the effective stresses (i.e. of the elastic strains).

At this stage of the research, the evolution laws of damage indexes are assumed similar to those proposed by Farja and Oliver (1998) and Saetta et al. (1999) and provided in Eqs. (5) and (6).

To complete the definition of the damage model the damage criterion has to be defined. Since we are dealing with an orthotropic material the damage surface cannot be defined in terms of principal stresses only, as for the classical isotropic ones, but also their orientations with respect to the material axes have to be kept into account. In this way, the damage surface can be expressed either in terms of ($\bar{\sigma}_1$, $\bar{\sigma}_2$, θ) or of the full effective stress vector ($\bar{\sigma}_x$, $\bar{\sigma}_y$ and $\bar{\tau}_{xy}$).

In this model the second representation has been chosen, since it is particularly appropriate for the proposed approach. The shape of this surface is a double pyramid with rectangular base, for which the slopes of the faces correspond to the internal friction angle of the material. In Fig. 2 the initial damage surface adopted for the analysis of the stack bond masonry is shown in the positive space $\bar{\tau} \geqslant 0$.

It is worth noting to observe that the shape of the damage surface together with the adoption of four independent damage variables allows to consider the biaxial problem as two uncoupled uniaxial problems

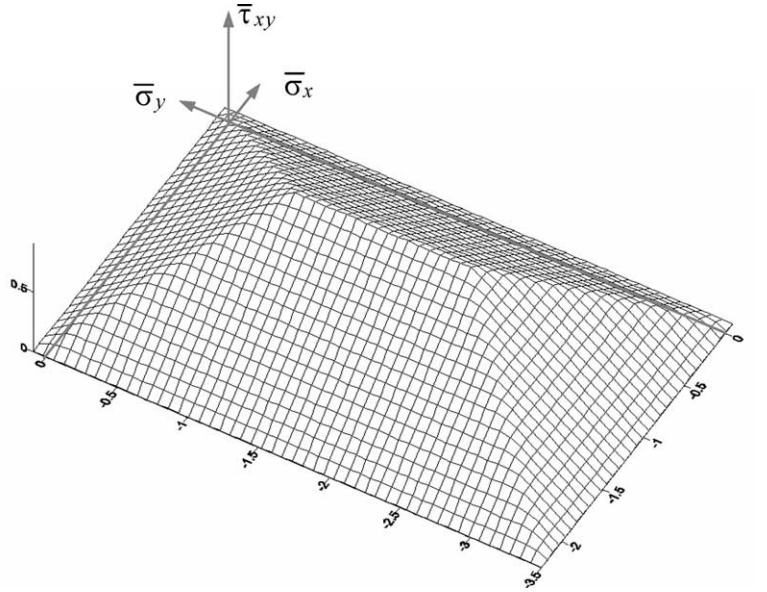

Fig. 2. Damage surface of the orthotropic damage model for the stack bond masonry in the space ($\bar{\sigma}_x$, $\bar{\sigma}_y$ and $\bar{\tau}_{xy}$) with $\bar{\tau}_{xy} \geqslant 0$ (in MPa).

(along the x and the y direction), each one with its own damage criteria (one for tension and one for compression). In such a way no complications in the damage variables updating occurs at the singular points of the damage surface.

Finally, in order to take into account the experimentally observed shear transmission capacity due to the friction phenomena through an open crack, a residual shear τ_{att} has been introduced depending on the existing level of compression and on a friction factor f, Berto et al. (2001):

$$\tau_{att} = \frac{|\langle -(\sigma_x + \sigma_y)\rangle|}{2} f \tag{9}$$

where the symbol $\langle\cdot\rangle$ indicates the MacAuley brackets.

In such a way a minimum for the shear strength is assured even for a completely damaged material, provided that the hydrostatic stress component be compression.

The detailed theories (with all the formulas and graphs) of the two formulations can been found in (Saetta et al., 1999) and (Berto et al., 2002) respectively.

2.3. Numerical details and mesh dependency

Both models have been implemented in a novel computer code in FORTRAN programming language.

The dependence of the damage parameters (that is of the stiffness matrix) on the strain tensor (that is on the displacement vector) leads to a solution of a system of non-linear equations. In these numerical applications the modified Newthon–Raphson scheme, with the initial stiffness matrix in place of the Jacobian matrix, is applied since it requires a reduced computational effort and assures a satisfactory stability and accuracy to the numerical solution.

The mesh dependency associated to the strain softening in a local finite element formulation has been partially overcome by adopting a simplified regularization approach. This method consists in linking the specific fracture energy to the size of the mesh element (Saetta et al., 1999). By following such an approach, the expression of the parameter A^+, which appears in (5), is:

$$A^+ = \left(\frac{G_f E_0}{l_c^{(e)} (f_t)^2} - \frac{1}{2} \right)^{-1} \tag{10}$$

where G_f is the fracture energy of the material, E_0 and f_t are, respectively, its initial Young's modulus and its tensile strength and $l_c^{(e)}$ is a characteristic length depending on the size of every finite element used in the FE mesh.

Since in this work only bi-dimensional cases are considered, the following expression for $l_c^{(e)}$ can be adopted:

$$l_c^{(e)} = \sqrt{A^{(e)}} \tag{11}$$

where $A^{(e)}$ is the element area.

2.4. Model validation

In the following the numerical analysis of a wall tested at ETH Zurich (Ganz and Thurlimann, 1984) will be proposed to validate the orthotropic model. Other validation examples can be found in Berto et al. (2002) and Berto et al. (2001). In particular good results had been found by simulating the experimental tests on masonry panels subjected to shear and compression carried out by Calvi et al. (1992) at the University of Pavia (Berto et al., 2002; Magenes and Calvi, 1997).

As shown in Fig. 3, the tested wall consists of a masonry panel and two lateral flanges, at the top and bottom of them are placed two concrete slabs. The wall has been firstly subjected to a vertical uniformly distributed load $p = 1.91$ MPa, in addition to the self weight, then a horizontal monotonically increased force has been applied on the top slab under displacement control.

Table 1 shows the mechanical parameters used in the numerical analysis, they are derived from the biaxial tests carried out from Ganz and Thurlimann (1982) and simulated by Lourenço (1996). The friction factor has been assumed equal to 0.7. As made by Lourenço in his analysis, we have assumed for the flanges in the x direction the tensile and compressive strength of the clay brick ($f_{tx} = 0.68$ MPa $f_{cx} = 9.5$ MPa). A regular mesh, made up of linear triangular elements, has been used.

The numerical load versus displacement curve is plotted in Fig. 4. and compared with the experimental one. A reasonably good agreement has been found.

Fig. 5 shows the damage contours for a displacement close to the experimental peak load (6.0 mm). It can be seen that at this displacement level the wall shows a diffuse tensile damage distribution d_x^+, in quite good agreement with the experimental crack pattern shown in Fig. 6, while the corresponding compressive damage, although already visible, is sufficiently low with respect to its limit value. At collapse the damage contours and the deformed configuration are shown, respectively, in Fig. 7 and Fig. 8. As evidenced by the

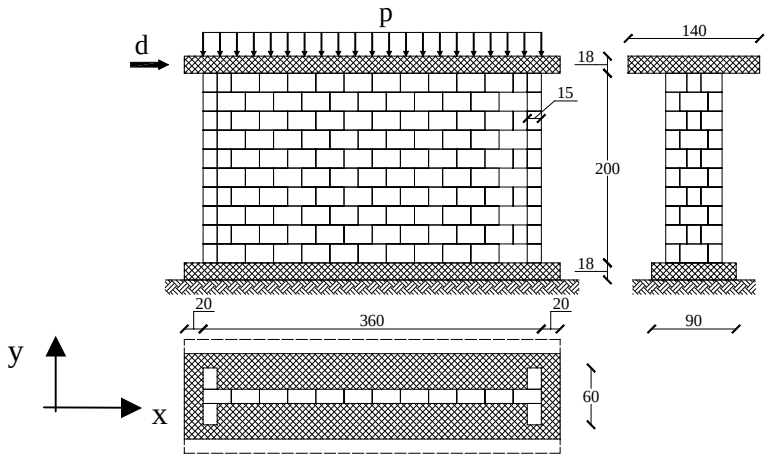

Fig. 3. ETH Zurich shear wall: geometry and loads (in cm).

Table 1
ETH Zurich shear wall: material's parameters for the macro-model

	x direction	y direction
Elastic modulus (MPa)	$E_x = 2460$	$E_y = 5460$
Shear modulus (MPa)	$G_{xy} = 1130$	
Poisson's ratio	$\nu_{xy} = 0.18$	
Uniaxial elastic limit in compression (MPa)	$f_{cx0} = 0.56$	$f_{cy0} = 1.37$
Uniaxial initial tensile strength (MPa)	$f_{tx} = 0.28$	$f_{ty} = 0.05$
Shear strength (MPa)	$f_\tau = 0.3$	
Fracture energy (N/mm)	$G_{fx} = 0.02$	$G_{fy} = 0.02$
A parameter	$A_{cx} = 0.12$	$A_{cy} = 0.24$
B parameter	$B_{cx} = 1.0$	$B_{cy} = 2.58$
Friction factor f (MPa)	$f = 0.7$	

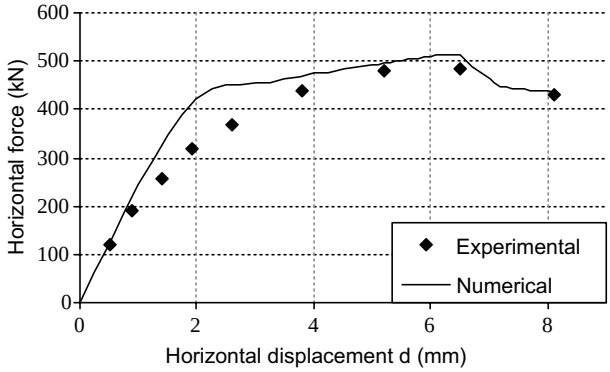

Fig. 4. Load–displacement diagrams: comparison between numerical and experimental results.

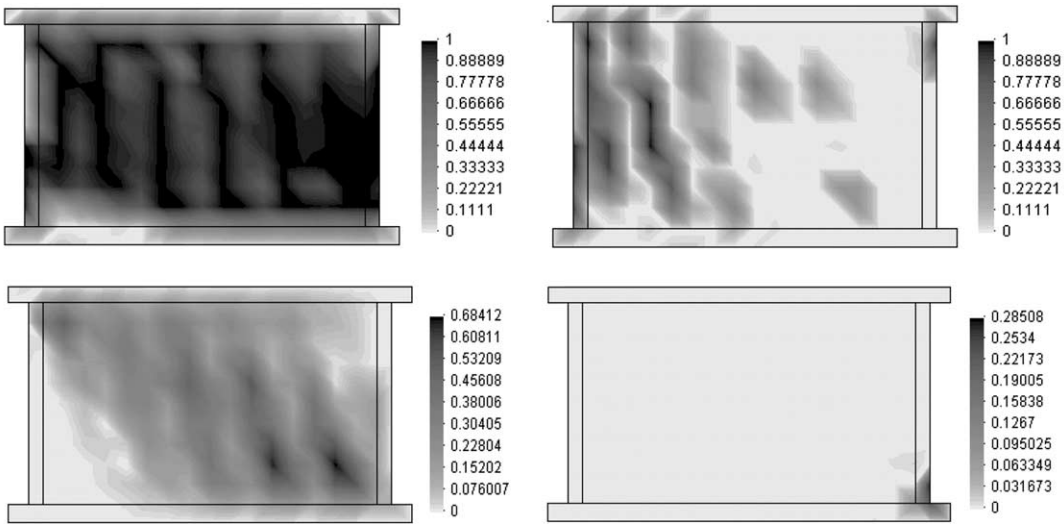

Fig. 5. Damage contours at the displacement of 6.0 mm.

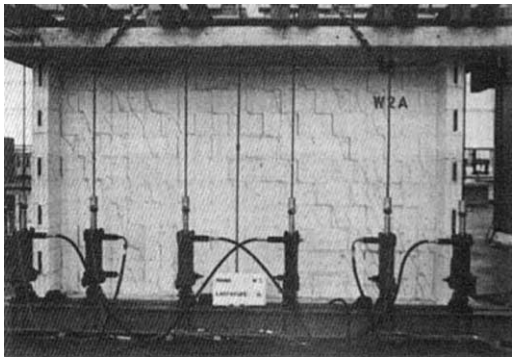

Fig. 6. ETH Zurich shear panel: experimental crack patterns at the displacement of 6.0 mm.

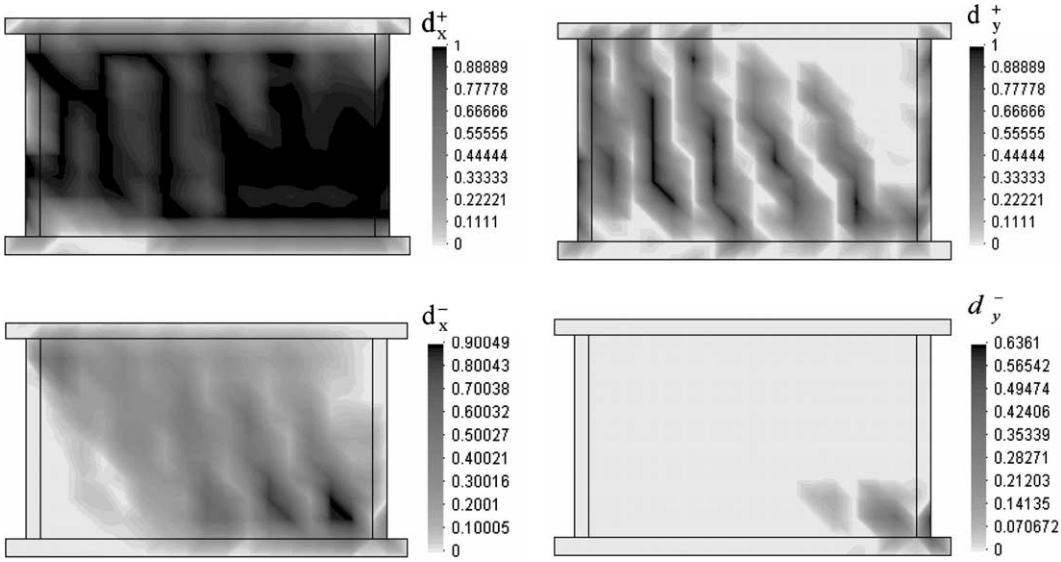

Fig. 7. Damage contours at the displacement of 8.0 mm (end stage).

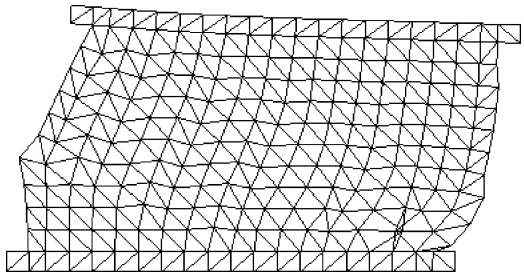

Fig. 8. Deformed configuration at the displacement of 8.0 mm (end stage).

significant development of compressive damage, the failure is dominated by masonry crushing in accordance with the experimental evidence (Fig. 9).

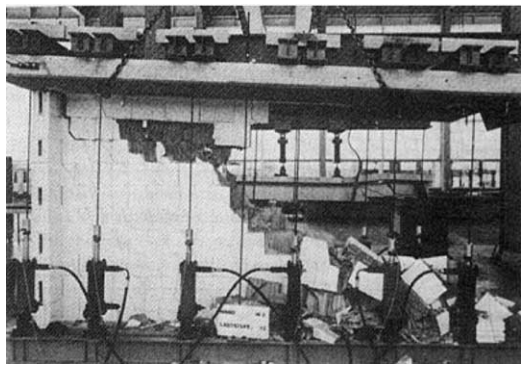

Fig. 9. ETH Zurich shear panel: experimental crack patterns at the displacement of 8.0 mm (end stage).

3. Effect of the texture on the shear behaviour of masonry panels

The aim of this first analysis is to capture and specifically understand the effect of the texture (that is stack bond or running bond) on the shear behaviour of masonry panels (Fig. 10). In such a preliminary analysis, a simplified mechanical model is adopted for which the blocks are modelled as rigid body and the mortar as an elastic material.

This hypothesis, together with the assumption of a macroscopically homogeneous shear state and a regular geometry, may refer this case to the Mann and Müller's theory (i.e. Mann and Müller, 1982). According to such an approach, the deformed configuration of the masonry panel is characterised by an identical rigid rotation of all the bricks and a deformation of the mortar joints.

The mechanical response of the two kind of masonry can be interpreted as depicted in Fig. 11, where the forces transmitted to a typical block by the surrounding mortar joints are evidenced (in the figure H and L are, respectively, the height and the width of the block).

In the case of running bond masonry, the shear stresses in the head joints are lower than those in the bed joints and the rotational equilibrium of the rigid block is ensured by the couples of the forces N (as indicated in Fig. 11b) according to the balance equation:

$$2N\frac{L}{2} + TL = \tau LH \tag{12}$$

Hence

$$N + T = \tau H \Rightarrow T < \tau H \tag{13}$$

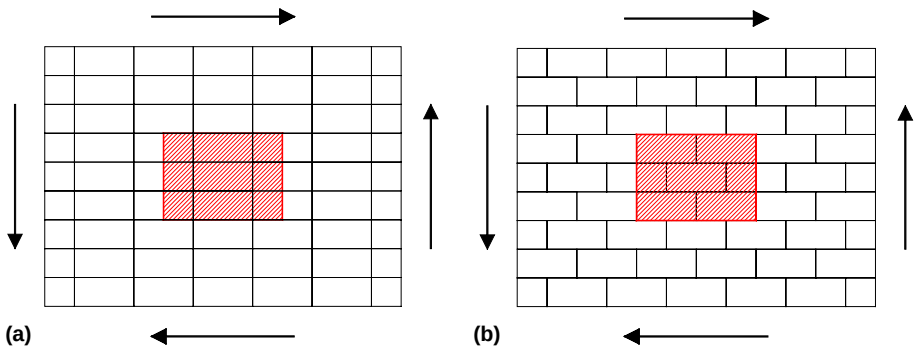

Fig. 10. Shear test on a masonry panel: (a) stack bond masonry and (b) running bond masonry.

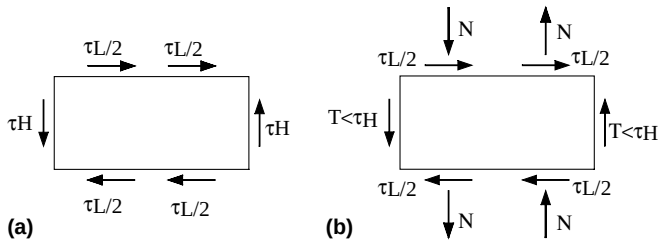

Fig. 11. Schematic representation of the forces transmitted to a typical block by the surrounding mortar joints: (a) stack bond masonry and (b) running bond masonry.

whereas for the stack bond masonry, for which the shear stresses in the head and in the bed joints are the same, the balance equation leads to

$$T = \tau H \tag{14}$$

It follows that when the head joints are completely cracked, the running bond masonry will be still able to withstand shear stresses and its shear modulus won't vanish unlike the stack bond masonry, for which the shear stresses in the head joints are essential to the rotational equilibrium.

The relevance of such a consideration is emphasised by the fact that, in real masonry structures, the vertical mortar joints are usually not well filled and that they are usually cracked because of the shrinkage.

Therefore all the methods developed to analyse the real response of masonry panel under shear loading condition should consider the effect of the damage in the mortar joint, at least in term of reduction of mechanical properties. The proposed analyses are aimed to give a contribution to the understanding and the effective representing of such a phenomenon, as well as to evaluate the effect of an applied vertical precompression to the panel.

Actually an initial prestressing improves the carrying behaviour by enhancing the friction force on the bed joints. According to the Coulomb's criterion, the shear strength increases as the axial compression ratio increases, and the correlated curve of combined shear compression stresses is uniformly ascending.

4. Numerical modelling

4.1. Micro-modelling

Following the micro-modelling approach, a first set of numerical analyses has been carried out with the aim of accurately capturing the local response of the masonry panels depicted in Fig. 10, under shear loading conditions: e.g. the effect of the texture (namely stack bond or running bond) and of an applied external precompression, as well as of following the evolution of damage growth in the mortar joints.

The parallel goals to obtain an effective simulation and to reduce as much as possible the computational complexity of the analyses, have led to consider only the central part of the panels (dashed in Fig. 10) by imposing appropriate boundary conditions. All the analyses are performed in plane stress hypothesis and under a displacement-controlled shear test.

The adopted mesh is depicted in Fig. 12 for both cases of stack and running bond masonry. Almost 1500 three-noded triangular elements are used.

The aim of the following analyses is to simulate the state of the panels, made by bricks geometrically identical and much stiffer than mortar, with a macroscopically homogeneous stress–strain shear state (i.e. Mann and Müller, 1982). Therefore the boundary conditions of the selected finite element meshes have to

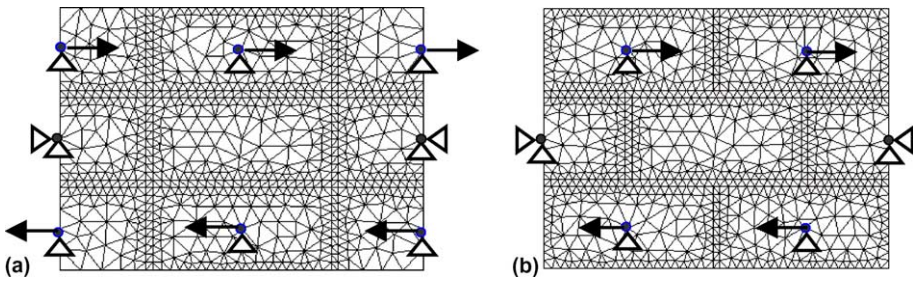

Fig. 12. Mesh adopted and imposed boundary conditions for the FE analysis: (a) stack bond masonry and (b) running bond masonry.

be imposed in such a way that all the blocks show the same rigid rotation. In the same Fig. 12 the constraint conditions and the imposed horizontal displacements used to simulate such a shear state are represented.

The brick dimensions are $250\times120\times125$ mm^3 (length × height × width) and the mortar thickness equals 10 mm.

For the units, a rigid model has been assumed, whereas for the mortar two different constitutive laws have been used: a linear elastic behaviour and a non-linear behaviour (Fig. 13) derived by the above-mentioned isotropic damage model. The parameters used to characterise the mortar material are summarised in Table 2.

For each type of texture the following numerical tests have been carried out:

- Shear test without an initial applied precompression by assuming a linear elastic behaviour for the mortar.
- Shear test without an initial applied precompression by assuming a non-linear elastic behaviour for the mortar.
- Shear test with an initial applied precompression $\sigma_y = 1$ MPa by assuming a non-linear elastic behaviour for the mortar.
- Shear test with an initial applied precompression $\sigma_y = 2$ MPa by assuming a non-linear elastic behaviour for the mortar.

4.1.1. Linear elastic analysis: comparison with the homogenization approach

The numerical results in terms of stresses due to a shear strain $\gamma = 1 \times 10^{-4}$, which rise in the mortar joints surrounding the central unit are represented in Figs. 14 and 15, respectively, for the stack and the running bond panel.

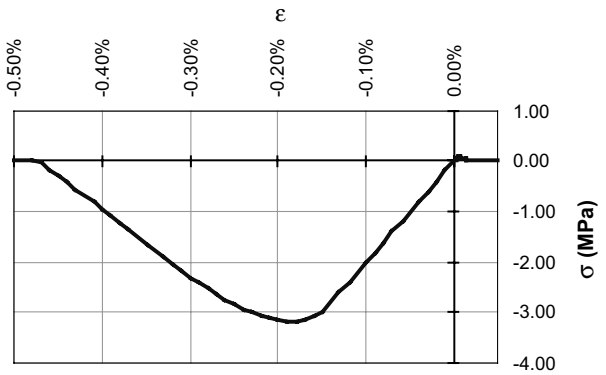

Fig. 13. Non-linear constitutive law for mortar.

Table 2
Mortar parameters for the elastic and isotropic damage model

Elastic modulus	$E = 2000$ MPa
Poisson's ratio	$v = 0.3$
Uniaxial elastic limit in compression	$f_c = 5.0$ MPa
Uniaxial initial tensile strength	$f_t = 0.1$ MPa
Fracture energy	$G_f = 0.00015$ N/mm
A^- parameter	$A^- = 0.8$
B^- parameter	$B^- = 2.3$

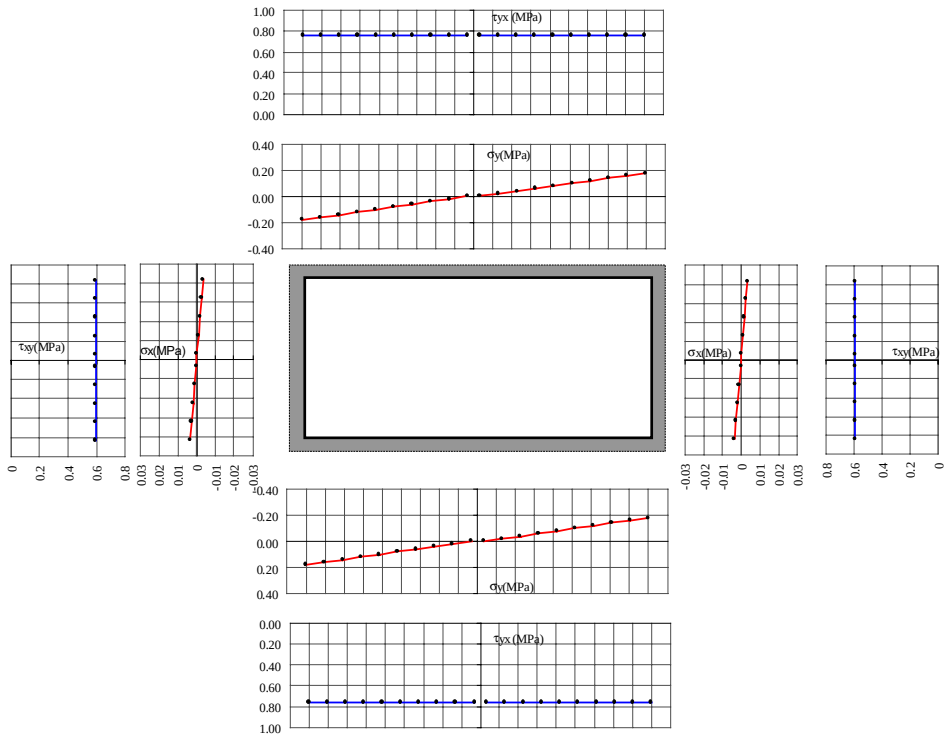

Fig. 14. Stack bond panel—diagram of the stresses in the mortar joints surrounding the central block for $\gamma = 1 \times 10^{-4}$.

As expected (see Section 3), in the case of stack bond the shear stresses are almost the same in the vertical joints and in the horizontal ones (0.6 versus 0.75 MPa). This slight difference can be ascribed to the fact that the applied numerical boundary conditions are not able to generate exactly the same rigid rotation to all the bricks, as can be noted by carefully looking at the deformed meshes (Fig. 16a). The unequal blocks rotations produce a triangularly distributed normal stresses, especially in the bed joints, whose contribution in the rotation equilibrium of the brick is only about 15% of the couple generated by the shear stresses. Therefore such an approximation does not dissimulate the ability of the model in describing the peculiar behaviour of the stack bond texture.

On the other hand, in the case of the running bond, the shear stresses are much lower in the head joints than in the bed ones (respectively, 0.33 and 0.85 MPa). Consequently not negligible normal stresses σ_y occur in the bed joints, inducing two significant couples of forces that ensure the rotational equilibrium of the rigid block. In particular, the moment of the couple in this case is four times as high as the one generated in the case of stack bond.

For each case a shear moduli G_{xy} can be evaluated as an *overall* parameter of the masonry panels. Such values can be compared with those obtained by applying the analytical formulae derived by Cecchi and Sab (2002) within the homogenization theory. They have provided an analytical expression of the homogenized stiffness tensor for stack and running masonry both for plane stress and for plane strain conditions in the hypothesis of small ratio of the mortar Young's modulus and the block Young's modulus and for small ratio of the joint thickness and block dimensions. By adopting these expressions in the stress plane condition in the hypothesis of infinitely stiff units, and assuming the elastic and the geometrical characteristics of the mortar joints and the blocks, the homogenized shear moduli for the two types of masonry has been obtained.

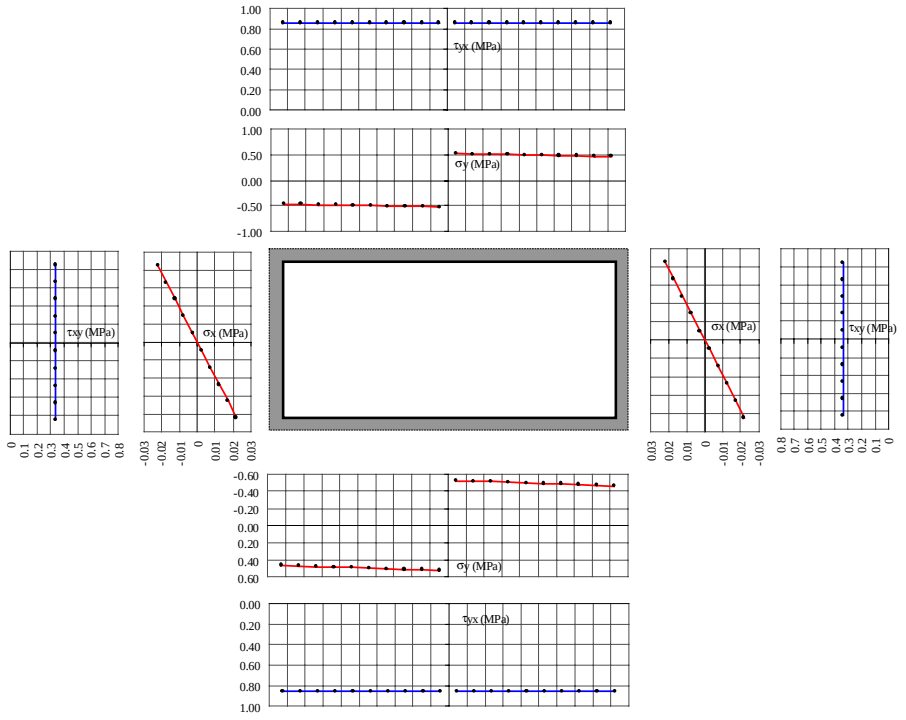

Fig. 15. Running bond panel—diagram of the stresses in the mortar joints surrounding the central block for $\gamma = 1 \cdot 10^{-4}$.

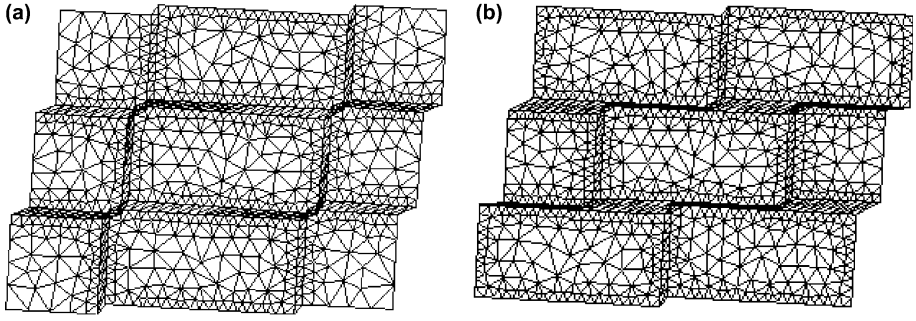

Fig. 16. Deformed mesh: (a) stack bond masonry and (b) running bond masonry.

The comparison between the results is proposed in Table 3, where the last column shows the percentage error e of the finite element solution with respect to the homogenization solution. As expected, the FE solutions reveal to be stiffer than the homogenization one; nevertheless the comparison is quite good especially for the running bond masonry.

4.1.2. Non-linear analysis—isotropic damage approach

In order to carry out some more information about the real shear behaviour of the masonry panels after the elastic range, the same tests have been repeated by assuming a non-linear constitutive law of the mortar via the isotropic damage approach. Within such an approach, the tensile strength of the mortar is assumed

Table 3
Comparison between the shear modulus derived from the homogenization theory and the FE linear elastic analysis

	Homogenization (MPa)	FE linear elastic analysis (MPa)	Percentual error (%)
Stack bond masonry	$G = 6235$	$G = 7820$	20
Running bond masonry	$G = 7735$	$G = 8615$	10

very low, so causing, as expected, a completely different stress distribution with respect to that obtained in the linear elastic hypothesis.

Fig. 17 shows the mechanical responses of the two masonry panels in terms of damage contours plotted for the same shear strain ($\gamma = 3 \times 10^{-5}$), next to the start of the inelastic behaviour. The effect of the different masonry texture is clearly evidenced: although the tensile damage starts to develop along the bed joints for both cases, the followed pattern is rather different. In the stack bond masonry, the tensile damage spreads along the bed joints almost instantly, then quickly along the head ones; whereas, in the running bond masonry, the damage at first affects the half part of the joints undergoing tensile stress and just after spreads along the whole mortar plane and then along the vertical joints.

The damage evolution can significantly change if an initial vertical precompression σ_y is applied to the panel. Actually, due to the vertical compression, for both the textures, the tensile damage firstly affects the head joints and only for high shear strain spreads to the horizontal ones.

Two different levels of precompression have been applied, respectively, $\sigma_y = 1$ MPa and $\sigma_y = 2$ MPa.

Figs. 18 and 19 show the damage contours for both study cases, plotted for a shear strain corresponding to an initial state of damage. It can be observed the well-known positive effect of an applied precompression, which for both the typologies of masonry leads to an expansion of the linear elastic range, even if with a different mechanism.

These observations are also legible in Fig. 20, where the global damage index is plotted versus the shear deformation γ. In such diagrams we can observe the shift of the tensile damage onset as the applied prestressing increases, particularly for the running bond masonry, whereas the compressive damage, which occurs firstly for the running bond masonry, shifts in the opposite side.

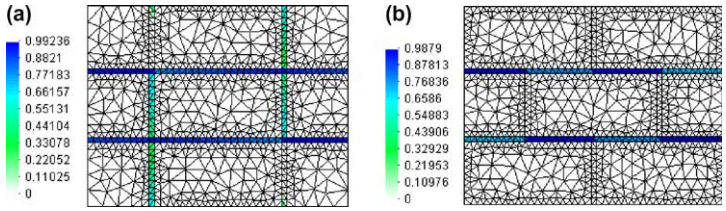

Fig. 17. Damage contours for $\gamma = 3 \times 10^{-5}$ without precompression: (a) stack bond masonry and (b) running bond masonry.

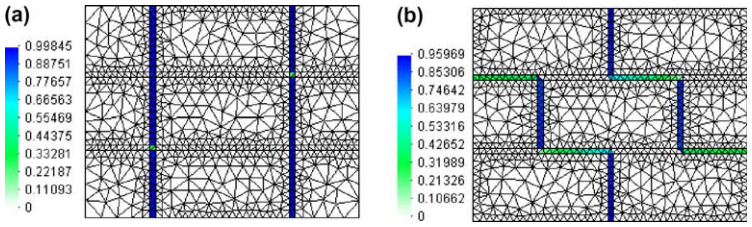

Fig. 18. Damage contours for $\gamma = 6 \times 10^{-5}$ with a precompression $\sigma_y = 1$ MPa: (a) stack bond masonry and (b) running bond masonry.

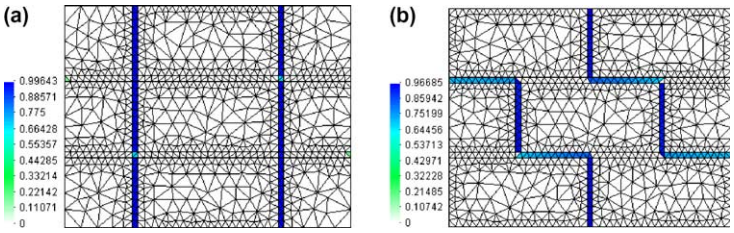

Fig. 19. Damage contours for $\gamma = 1.1 \times 10^{-4}$ with a precompression $\sigma_y = 2$ MPa: (a) stack bond masonry and (b) running bond masonry.

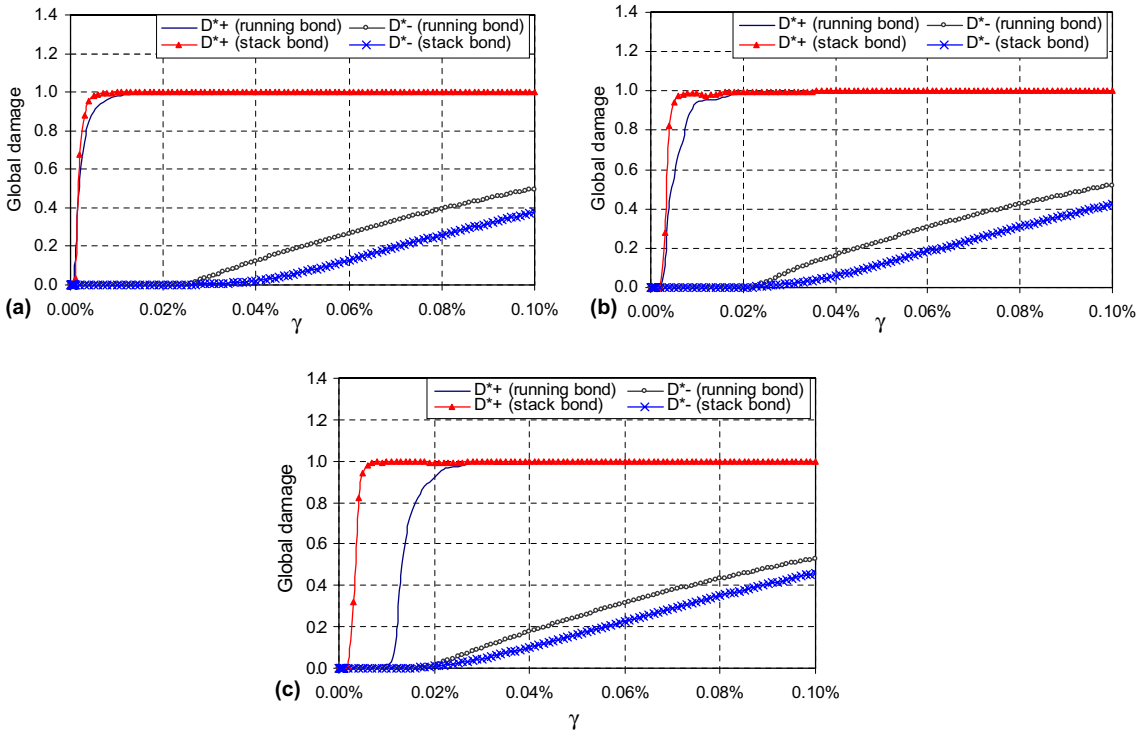

Fig. 20. Evolution of the tensile and compressive global damage indexes vs. the shear strain curves for running and stack bond masonry: (a) without precompression; (b) with precompression $\sigma_y = 1$ MPa and (c) with precompression $\sigma_y = 2$ MPa.

Finally in Figs. 21 and 22 the results in terms of τ–γ and σ_y–γ curves are given, respectively, for stack bond and running bond masonry. Some consideration and discussion will be proposed in the next section.

4.1.3. Discussion and remarks

Since we are dealing with displacement-controlled shear tests, as soon as the non-linear range is reached, the plain shear state (i.e. ε_x, $\varepsilon_y = 0$ and σ_x, $\sigma_y = 0$) is no more a maintainable state.

Actually, as the imposed displacements assigned to the central point of the units increases, we observe an increasing damage in the mortar joints, which causes an increasing compression state, as demonstrated by the diagrams of Fig. 21b and Fig. 22b. In other words, after the damage onset, the increasing shear strain involves increasing vertical forces in the centres of the upper and lower blocks, in order to respect the

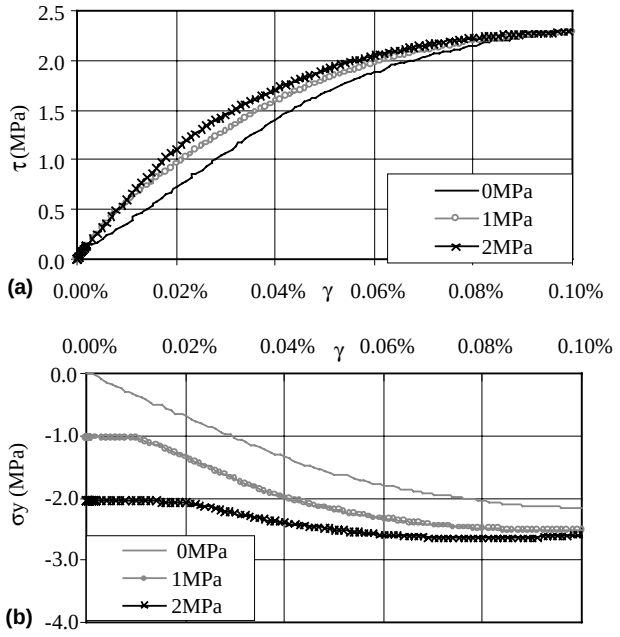

Fig. 21. Stack bond masonry: results for different values of applied prestressing: (a) τ–γ curves; (b) σ_y–γ curves.

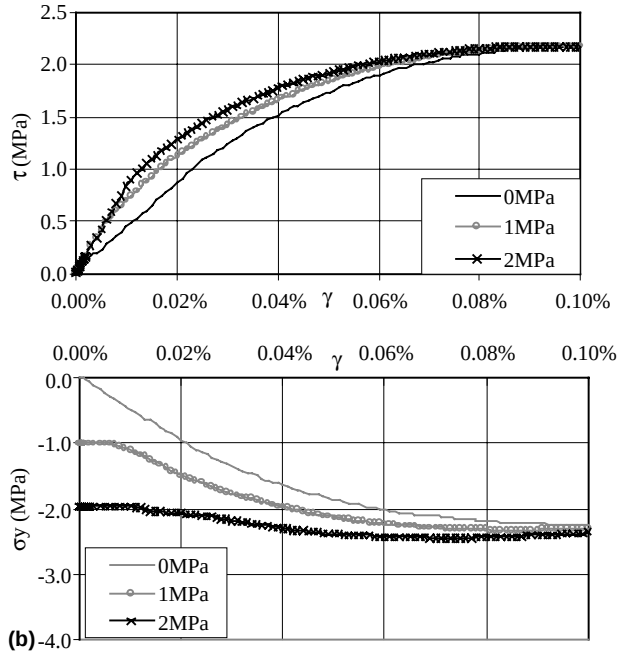

Fig. 22. Running bond panel: results for different values of applied prestressing: (a) τ–γ curves and (b) σ_y–γ curves.

equilibrium and continuity conditions, and therefore the ideal condition of the pure shear stress state $\sigma_y = 0$ is not more respected.

The same phenomenon occurs also in the non-linear analyses with an applied precompression. Therefore we have to refer to an "initial" or "nominal" precompression, since the real one goes up with the increasing of the damage.

With such a remark in mind, a comparison between the graphs drawn in Figs. 21(a) and 22(a) can now be made. In particular, the above-mentioned increasing internal compression justifies the same response that all the samples show for high shear strain, independently from the type of texture and the "initial" precompression level. Therefore the more significant results can be found in the initial parts of the graphs.

4.2. Macro-modelling

The second part of this paper is devoted to evaluate the effectiveness and potentiality of macro-modelling approach to treat the shear response of masonry panels. The main concern is to prove the capability of the orthotropic macro-model, which has been described in Section 2.2, to properly capture the global response of the shear stressed masonry panels, with a reduced computational effort.

To this aim a single four-noded finite element has been used to represent the same panels that had been studied in the previous section, e.g. Fig. 12. The orthotropic damage model is applied to each loading condition previously investigated with the micro-model approach.

The first step required to perform such analyses is the evaluation of all the mechanical parameters used by macro-model.

4.2.1. Orthotropic damage model calibration

Some preliminary considerations are needed to better illustrate the procedure used to evaluate the mechanical parameters necessary to apply the orthotropic damage model described in Section 2.2, starting from the results obtained with micro-modelling tests.

The macro-model, in its original formulation, needs four linear elastic parameters (E_x, E_y, G_{xy}, v_{xy}), and eleven non-linear parameters (f_{tx}, f_{ty}, f_{cx0}, f_{cy0}, f_τ; G_{fx}, G_{fy}, A_x^-, B_x^-, A_y^-, B_y^-).

The first group characterises the elastic behaviour of the orthotropic material in plane stress condition: respectively, the Young's moduli E_x, E_y along the two natural directions, the shear modulus G_{xy} and one Poisson's ratio v_{xy} (the other one, i.e. v_{yx}, can be derived from the relation $v_{xy}/E_x = v_{yx}/E_y$).

The second group refers to the strength and the non-linear behaviour of the material. Such parameters are respectively: the uniaxial tensile strengths f_{tx}, f_{ty} and the uniaxial compressive linear thresholds f_{cx0}, f_{cy0} along the material axes; the shear strength f_τ; the last six parameters characterise the shape of the non-linear part of the constitutive curve along the two directions, both in tensile field (i.e. the fracture energies G_{fx}, G_{fy}) and in the compressive one (i.e. the parameters A_x^-, B_x^-, A_y^-, B_y^-). All these parameters can be evaluated by performing the five tests schematically drawn in Fig. 23 under displacement controlled conditions.

The last parameter to be defined is the friction factor f, i.e. Eq. (9), for which one additional test has to be performed accounting for the contemporary presence of compression and shear.

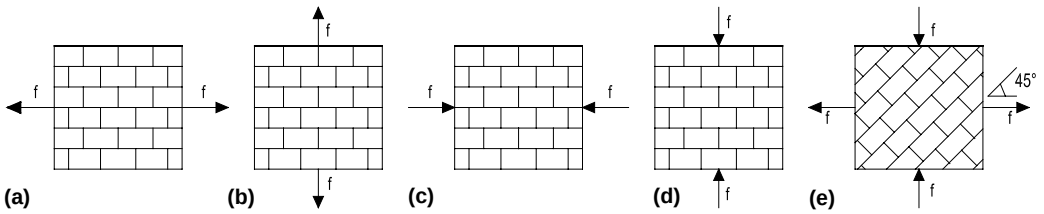

Fig. 23. Tests to calibrate the orthotropic damage model: (a) uniaxial tension parallel to the bed joints; (b) uniaxial tension normal to the bed joints; (c) uniaxial compression parallel to the bed joints; (d) uniaxial compression normal to the bed joints and (e) shear test.

Such tests can be carried out both via experimental as well as numerical way. However, since it is usually easier to get experimental data on the single components (i.e. mortar and bricks) than on a masonry panel, the numerical simulation is the more appealing technique. In particular two different approaches can be applied: homogenization techniques (useful to evaluate the elastic properties) and micro-modelling simulations, both based on the mechanical characteristics of the constituent materials.

In the present work, the latter procedure has been adopted and the mechanical parameters of the macro-model have been obtained by using the results of the previously described micro-modelling tests.

4.2.2. Comparison between the results of micro- and macro-modelling

Four additional numerical simulations have been carried out on both the masonry panels we have analysed in Section 4.1 (i.e. the running bond and the stack bond masonry): two uniaxial compressive tests and two uniaxial tensile tests, along the two material axes. The results have been summarised in Fig. 24 in terms of $\sigma - \varepsilon$ curves that have allowed to evaluate 13 of the material parameters requested by the macro-model, that is E_x, E_y, ν_{xy}, f_{tx}, f_{ty}, f_{cx0}, f_{cy0}, G_{fx}, G_{fy}, A_x^-, B_x^-, A_y^-, B_y^-.

For what concerns the shear behaviour of masonry (i.e. the estimation of the shear modulus G_{xy}, the shear strength f_τ, and the friction factor f) the tests developed in the previous section have been considered.

The simulation of these tests by using the single four-noded finite element has led to the estimation of all the macro-model properties, which are summarised in Tables 4 and 5, respectively, for the stack bond masonry and for the running bond masonry.

It is worth noting how the different texture reflects on different global behaviour of the panels and consequently on different values of macro-model properties, especially along the x-direction for which no interlock is active.

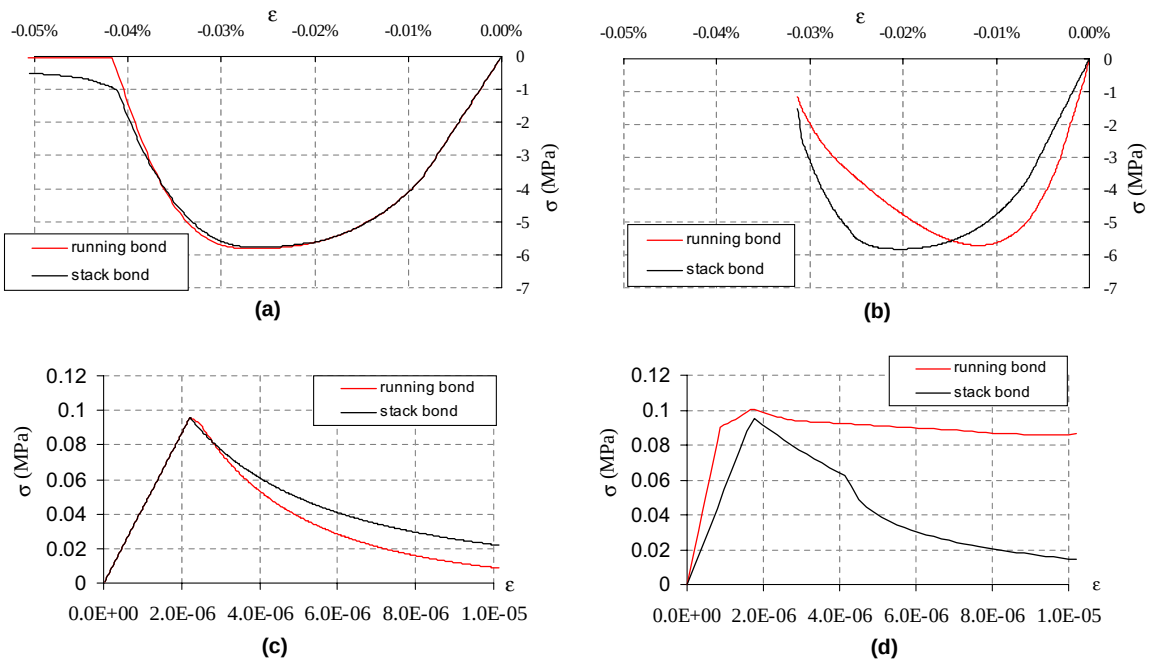

Fig. 24. Results of the numerical tests: (a) compression normal to the bed joints; (b) compression parallel to the bed joints; (c) tension normal to the bed joints and (d) tension parallel to the bed joints.

Table 4
Stack bond masonry

	x direction	y direction
Elastic modulus (MPa)	$E_x = 56000$	$E_y = 43000$
Shear modulus (MPa)	$G_{xy} = 7820$	
Poisson's ratio	$v_{xy} = 0.01$	
Uniaxial elastic limit in compression (MPa)	$f_{cx0} = 3.5$	$f_{cy0} = 2.25$
Uniaxial initial tensile strength (MPa)	$f_{tx} = 0.09$	$f_{ty} = 0.09$
Shear strength (MPa)	$f_\tau = 0.07$	
Fracture energy (N/mm)	$G_{fx} = 0.00007$	$G_{fy} = 0.00007$
A parameter	$A_{cx} = 0.4$	$A_{cy} = 0.2$
B parameter	$B_{cx} = 2.0$	$B_{cy} = 1.3$
Friction factor f (MPa)	$f = 0.65$	

Material's parameters for the macro-model.

Table 5
Running bond masonry

	x direction	y direction
Elastic modulus (MPa)	$E_x = 111000$	$E_y = 43000$
Shear modulus (MPa)	$G_{xy} = 8615$	
Poisson's ratio	$v_{xy} = 0.02$	
Uniaxial elastic limit in compression (MPa)	$f_{cx0} = 2.85$	$f_{cy0} = 2.25$
Uniaxial initial tensile strength (MPa)	$f_{tx} = 0.11$	$f_{ty} = 0.1$
Shear strength	$f_\tau = 0.08$	
Fracture energy (N/mm)	$G_{fx} = 0.00025$	$G_{fy} = 0.00005$
A parameter	$A_{cx} = 0.28$	$A_{cy} = 0.2$
B parameter	$B_{cx} = 1.5$	$B_{cy} = 1.3$
Friction factor f (MPa)	$f = 0.75$	

Material's parameters for the macro-model.

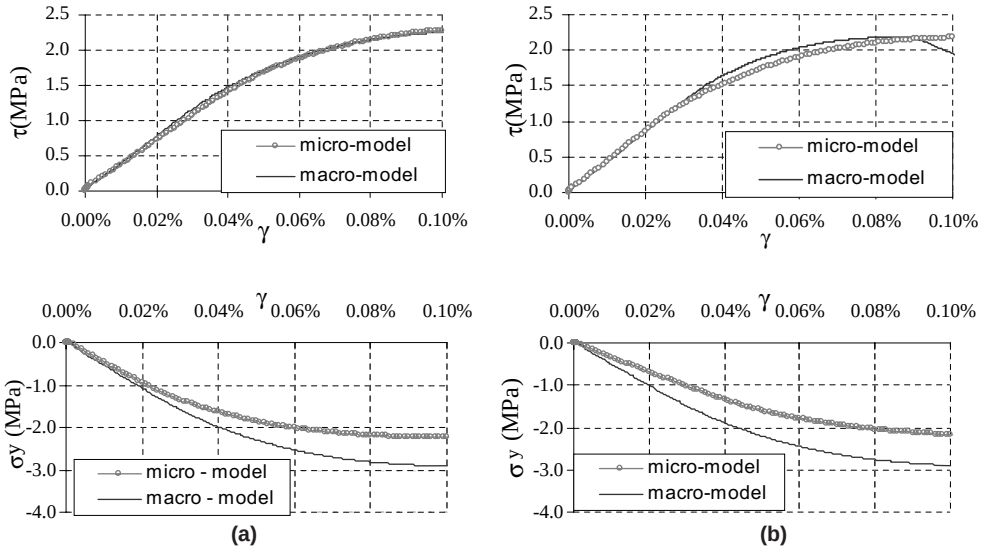

Fig. 25. Results of the numerical tests without "initial" precompression. τ–γ curves and σ–γ for the: (a) stack bond masonry and (b) running bond masonry.

Figs. 25–27, show the results of the macro-modelling both in terms of τ–γ curves and of σ–γ curves, respectively for the stack bond and the running bond masonry panels. In the same figures, the curves obtained with micro-modelling, i.e. Figs. 21 and 22, have been reproposed, in order to allow a more comprehensive explanation and presentation of the analyses results.

As previously stated within the framework of micro-modelling, it can be observed that in the non-linear field the increase of shear strain is accompanied by an increase of the precompression. It is worth recalling

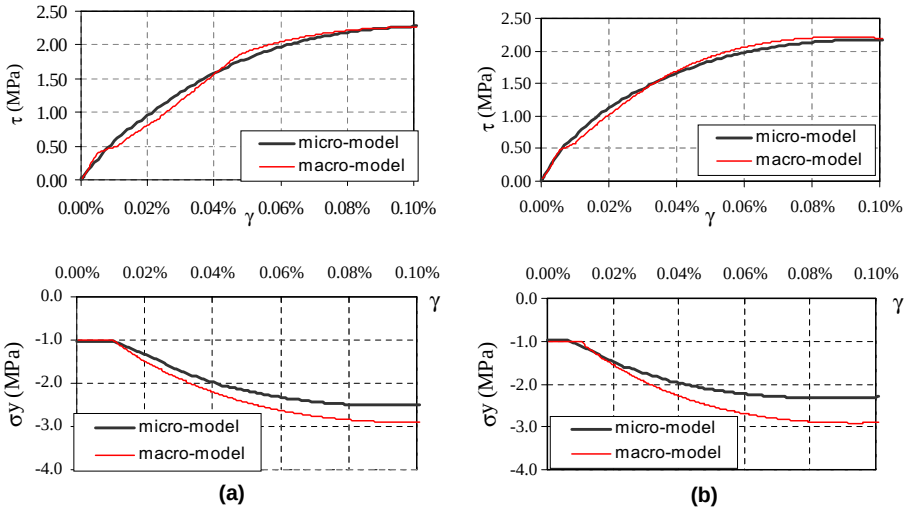

Fig. 26. Results of the numerical tests with "initial" precompression $\sigma = 1$ MPa. τ–γ curves and σ–γ for the: (a) stack bond masonry and (b) running bond masonry.

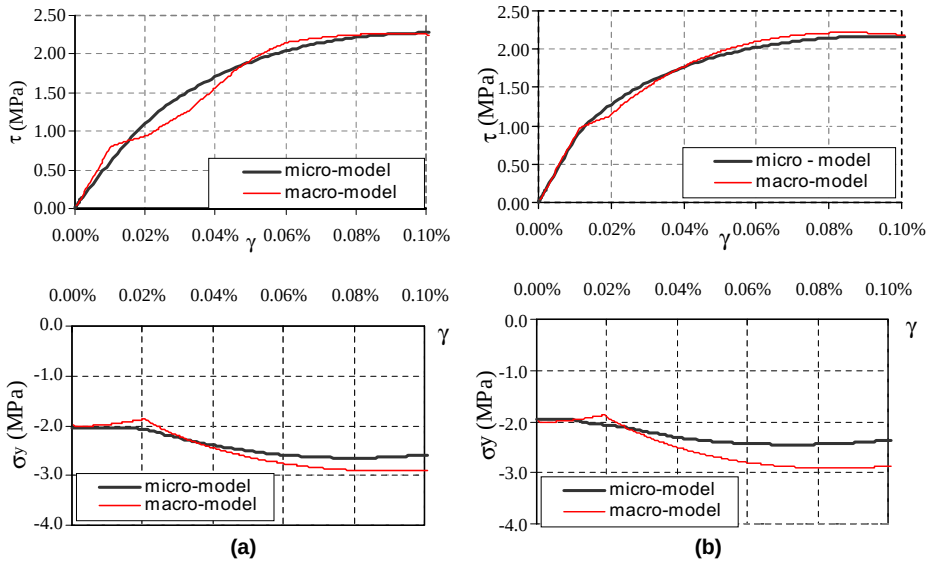

Fig. 27. Results of the numerical tests with "initial" precompression $\sigma = 2$ MPa. τ–γ curves and σ–γ for the: (a) stack bond masonry and (b) running bond masonry.

that such an effect can justify the same response that all the panels show for high shear strain, independently from the type of texture and the "initial" precompression level.

A good impression about the adequacy of the adopted orthotropic constitutive law to model masonry is obtained. Actually, with a single set of material parameters, the model reveals to be able to reproduce in a satisfactory way the shear behaviour of the panels both in the linear and in the non-linear field, also by gathering the effects of the masonry texture.

5. Conclusion

The shear behaviour of masonry panels has been analysed both by means of micro- and macro-finite element modelling. The effect of the texture (namely stack bond or running bond) and of an applied external precompression has been investigated.

In the first part the micro-modelling has been applied. First, a simple linear analysis is performed and the numerical results for the stack bond and running bond masonry are compared with those achieved by applying the homogenization theory, and satisfactory agreement has been found. Subsequently an isotropic damage model, which has been developed and validated in previous works, has been used in order to simulate the non-linear behaviour of masonry. In such a way the shear response of masonry besides the elastic range has been investigated. It is worth noting that the analysis of the non-linear response of masonry is quite difficult to gain by using the homogenization technique, whereas the employment of experimental tests requires high costs and very sophisticated experimental technique, e.g. due to the brittleness of the sample.

Such tests demonstrate the capability of the model to follow the evolution of mechanical response of masonry panels, both in linear and non-linear range, according to the intuitive results of the rigid blocks mechanical model, e.g. the effect of the texture in the stiffness and strength of shear stressed masonry, as well as the influence of an applied precompression.

In the second part of the paper an orthotropic damage model, specifically developed by the authors for analysing masonry structures, has been used. A fully characterisation of the macro-model, which takes into account both the effect of the texture and precompression, has been achieved by using the micro-modelling approach. The obtained results have demonstrated the ability of the macro-model of reproducing the global behaviour, as well as the failure modes of shear stressed masonry panel.

Such a result is very interesting for the practical application, since in this field the micro-modelling procedure is rarely applied because of the intensive computational effort its high accuracy required, and the macro-modelling procedure is the only effective option.

In this paper the use of the micro-modelling technique to determine the parameters necessary to calibrate a macro-model is shown and the effectiveness of the macro-model to capture the global shear behaviour of masonry is evidenced.

Acknowledgements

The authors would like to express their thanks to prof. Antonio Di Carlo for his helpful advice in the preparation of this paper and dr. Antonella Cecchi for valuable discussions.

References

Ali, S.S., Page, A.W., 1988. Finite element model for masonry subjected to concentrated loads. J. Struct. Eng. 114 (8), 1761–1784.
Andreaus, U., 1996. Failure criteria for masonry panels under in-plane loading. J. Struct.Eng., ASCE 122 (1).

Asteris, P.G., Tzamtzis, A.D., 2003. On the use of a regular yield surface for the analysis of unreinforced masonry walls. Electron. J. Struct. Eng. 3, 23–42, Available from <http://www.ejse.org>.

Berto, L., Saetta, A., Scotta, R., Vitaliani, R., 2001. An orthotropic damage model for non-linear masonry walls analysis: irreversible strain and friction effects. In: Proceedings of the III International Seminar Structural Analysis of Historical Construction, 7–9 November.

Berto, L., Saetta, A., Scotta, R., Vitaliani, R., 2002. An orthotropic damage model for masonry structures. Int. J. Numer. Method Eng. 55 (22), 127–157.

Callerio, A., Papa, E., 1998. An elastic–plastic model with damage for cyclic analysis of masonry panels. In: Pande, Middleton, Kralj, (Eds.), Computer Methods in Structural Masonry-4. E&FN Spon, London.

Calvi, M., Magenes, G., Pavese, A., 1992. Indagine sperimentale e numerica su un prototipo di edificio in muratura. CNR GNDT, Doc. 1.1., 1992 (in Italian).

Cecchi, A., Sab, K., 2002. A multi-parameter homogenization study for modelling elastic masonry. Eur. J. Mech. A—Solids 21, 249–268.

Farja, R., Oliver, J., 1998. A strain-based viscous-plastic-damage model for massive concrete structures. Int. J. Solids Struct. 35, 1533–1558.

Fonseka, G.U., Krajcinovic, D., 1981. The continuous damage theory of brittle materials—Part 2: general theory. J. Appl. Mech., Trans. ASME 48, 816–824.

Gambarotta, L., Lagomarsino, S., Morbiducci, R., 1995. Two-dimensional finite element simulation of a large scale brick masonry wall through a continuum damage model. Experimental and numerical investigation on a brick masonry building prototype, Report 3.0, CNR GNDT.

Ganz, H.R., Thurlimann, B., 1982. Tests on biaxial strength of masonry. Report No.7502-3. ETH Zurich Institute of Structural Engineering, Zurich (in German).

Ganz, H.R., Thurlimann, B., 1984. Tests on masonry walls under normal and shear loading. Report No.7502-4. ETH Zurich Institute of Structural Engineering, Zurich (in German).

Lofti, H.R., Shing, B.P., 1994. Interface model applied to fracture of masonry structures. J. Struct. Eng., ASCE 120 (1), 63–80.

Lourenço, P.B., 1996. Computational Strategies for Masonry Structures. Delft University Press, Delft, The Netherlands.

Magenes, G., Calvi, M., 1997. In plane seismic response of brick masonry walls. Earth. Eng. Struct. Dyn. 26, 1091–1112.

Mann, W., Müller, H., 1982. Failure of shear-stressed masonry—an enlarged theory, tests and application to shear walls. In: West, H.W.H., (Ed.), Proceedings of the British Ceramic Society, No. 30, September.

Massart, Th., Bouillard, Ph., Geers, M.G.D., Peerlings, R.H.J., 2001. A 2D Anisotropic damage model for masonry walls. In: Procedings of V European Conference on Computational Mechanics, Cracow, Poland.

Oñate, E., 1994. Reliability analysis of concrete structures. Numerical and experimental studies. In: Evoluzione nella sperimentazione per le costruzioni, Seminar CISM, Merano, Italy, pp. 125–146.

Page, A.W., 1978. Finite element model for masonry. J. Struct. Div., ASCE 104 (ST8), 1267–1285.

Papa, E., Nappi, A., 1996. Modellazione numerica di strutture murarie soggette a carichi ciclichi. In: Gambarotta, L. (Ed.), La meccanica delle murature tra teoria e progetto. Proceedings of the National Conference, Messina, Italy, pp. 441–450.

Saetta, A., Scotta, R., Vitaliani, R., 1999. Coupled environmental–mechanical damage model of RC structures. J. Eng. Mech., ASCE 125 (8), 930–940.

Simo, J.C., Ju, J.W., 1987. Strain and stress based continuum damage models—part I: formulation. Int. J. Solids Struct. 23 (7), 821–840.

Sutcliffe, D.J., Yu, H.S., Page, A.W., 2001. Lower bound limit analysis of unreinforced masonry shear walls. Comput. Struct. 79, 1295–1312.

Syrmakezis, C.A., Asteris, P.G., 2001. Masonry failure criterion under biaxial stress state. J. Mater. Civil Eng. 13 (1), 58–64.

Tzamtzis, A.D., 1994. Dynamic finite element analysis of complex discontinuous and jointed structural systems using interface elements. Ph.D. Thesis, Department of Civil Engineering, QMWC, University of London.

Zhuge, Y., Thambiratnam, D., Corderoy, J., et al., 1998. Non-linear dynamic analysis of un-reinforced masonry. J. Struct. Eng., ASCE 124 (3), 270–277.

Zucchini, A., Lourenço, P.B., 2002. A micro-mechanical for the homogenisation of masonry. Int. J. Solids Struct. 39, 3233–3255.